AFRL-RZ-WP-TP-2012-0152

FLUX PINNING ENHANCEMENT IN YBa$_2$Cu$_3$O$_{7\text{-}x}$ FILMS FOR COATED CONDUCTOR APPLICATIONS (POSTPRINT)

C.V. Varanasi

University of Dayton Research Institute

P.N. Barnes

Mechanical Energy Conversion Branch
Energy/Power/Thermal Division

FEBRUARY 2012

STINFO COPY

AIR FORCE RESEARCH LABORATORY
PROPULSION DIRECTORATE
WRIGHT-PATTERSON AIR FORCE BASE, OH 45433-7251
AIR FORCE MATERIEL COMMAND
UNITED STATES AIR FORCE

REPORT DOCUMENTATION PAGE

Form Approved
OMB No. 0704-0188

1. REPORT DATE *(DD-MM-YY)*	2. REPORT TYPE	3. DATES COVERED *(From - To)*
February 2012	Journal Article Postprint	01 May 2007 – 01 May 2009

4. TITLE AND SUBTITLE
FLUX PINNING ENHANCEMENT IN $YBa_2Cu_3O_{7-x}$ FILMS FOR COATED CONDUCTOR APPLICATIONS (POSTPRINT)

5a. CONTRACT NUMBER
In-house

5b. GRANT NUMBER

5c. PROGRAM ELEMENT NUMBER
62203F

6. AUTHOR(S)
C.V. Varanasi (University of Dayton Research Institute)
P.N. Barnes (AFRL/RZPG)

5d. PROJECT NUMBER
3145

5e. TASK NUMBER
32

5f. WORK UNIT NUMBER
314532ZE

7. PERFORMING ORGANIZATION NAME(S) AND ADDRESS(ES)

University of Dayton Research Institute
300 College Park
Dayton, OH 45469

Mechanical Energy Conversion Branch (AFRL/RZPG)
Energy/Power/Thermal Division
Air Force Research Laboratory, Propulsion Directorate
Wright-Patterson Air Force Base, OH 45433-7251
Air Force Materiel Command, United States Air Force

8. PERFORMING ORGANIZATION REPORT NUMBER
AFRL-RZ-WP-TP-2012-0152

9. SPONSORING/MONITORING AGENCY NAME(S) AND ADDRESS(ES)

Air Force Research Laboratory
Propulsion Directorate
Wright-Patterson Air Force Base, OH 45433-7251
Air Force Materiel Command
United States Air Force

10. SPONSORING/MONITORING AGENCY ACRONYM(S)
AFRL/RZPG

11. SPONSORING/MONITORING AGENCY REPORT NUMBER(S)
AFRL-RZ-WP-TP-2012-0152

12. DISTRIBUTION/AVAILABILITY STATEMENT
Approved for public release; distribution unlimited.

13. SUPPLEMENTARY NOTES
Journal article published as a chapter in High Temperature Superconductors. © 2010 Wiley-VCH. The U.S. Government is joint author of this work and has the right to use, modify, reproduce, release, perform, display, or disclose the work. PA Case Number: 88ABW-2009-2167; Clearance Date: 01 May 2009.

14. ABSTRACT
It is shown that YBCO films with $BaSnO_3$ (BSO) nano-additions, made with either a sectored target or with a premixed target using pulsed-laser deposition (PLD), have a much greater improvement in J_c at the higher fields with an H//c orientation. More than two orders of magnitude improvement in J_c was observed as compared to undoped or similarly processed Y_2BaCuO_5 (Y211) doped samples at magnetic fields higher than 5 T. The improvement was found to be due to the formation of BSO nanocolumns 8–10 nm in diameter in the films. These nanocolumns nucleate at the interface and subsequently grow perpendicular to the substrate while allowing high-quality YBCO to grow around them. Although similar processing conditions were used, Y211 formed nanoparticles, whereas BSO formed nanocolumns in the YBCO because of the crystal structure match between BSO and YBCO (both are perovskites) and appropriate lattice strain and suitable deposition conditions. The BSO content was also systematically increased from 2 to 20 mol% by using premixed targets of YBCO and BSO to explore the effects of BSO content variation in YBCO. It was shown that even with 20 mol% BSO addition; films can be grown without a significant decrease in critical transition temperature (T_c). While the diameter of the nanocolumns remained at 8–10 nm, the distance between them decreased from 50 nm to 20 nm as the concentration was increased from 2 mol% to 20 mol%, resulting in an increase in the number density. An overall improvement at both low and high fields was observed in samples of YBCO+10 mol% BSO. The YBCO+BSO films deposited on buffered metallic substrates showed improvements as seen on the single-crystal substrates, indicating that the BSO nano-additions can be introduced on polycrystalline buffer layers as used in coated conductors. Unlike $BaZrO_3$, BSO seems to allow higher relative amounts of additions to YBCO without significantly depressing the T_c value. The BSO nanocolumns seem to grow as solid nanorods as opposed to stacked individual nanoparticles. In addition, they were found to grow vertically straight and hence help to improve the J_c at high fields by several orders of magnitude in thick films making BSO attractive for coated conductors.

15. SUBJECT TERMS flux pinning enhancement, artificially introduced defects, barium-tin oxide (BSO), crystalline defects, microstructural defects, rare earth doping, second-phase additions, pulsed-laser deposition, alternate targets, pre-mixed targets, layered targets

16. SECURITY CLASSIFICATION OF:			17. LIMITATION OF ABSTRACT:	18. NUMBER OF PAGES	19a. NAME OF RESPONSIBLE PERSON (Monitor)
a. REPORT	**b. ABSTRACT**	**c. THIS PAGE**	SAR	30	Timothy J. Haugan
Unclassified	Unclassified	Unclassified			19b. TELEPHONE NUMBER (Include Area Code) N/A

Standard Form 298 (Rev. 8-98)
Prescribed by ANSI Std. Z39-18

5

Flux Pinning Enhancement in YBa$_2$Cu$_3$O$_{7-x}$ Films for Coated Conductor Applications

C.V. Varanasi and P.N. Barnes

5.1
Introduction

Coated conductors are electrical conductors prepared with YBa$_2$Cu$_3$O$_{7-x}$ (YBCO) superconducting material coatings deposited on metallic substrates along with several other intermediate buffer layers. Buffer layers are deposited sequentially on the metallic substrates prior to YBCO deposition to serve as barrier layers. They are selected such that epitaxial relationships are maintained throughout the thickness of the coated conductors to obtain highly-textured YBCO coatings. To process conductors with high critical current density (J_c), highly-textured YBCO coatings with both in-plane and out-of-plane alignment of grains are required with grain boundary misorienation angles below 5°. More details of the texture requirements, processing, and different types of coated conductor architectures can be found in other chapters of this book as well as in the references [1–5]. Two primary industrial approaches are used to manufacture the coated conductors. One approach uses a rolling assisted biaxially textured (RABiTS™) metallic substrate such as N-5 at.% W with sputtered Y$_2$O$_3$/YSZ/Ce$_2$O$_3$ buffer layers and YBCO layer deposited by the metallo-organic deposition (MOD) technique [3]. In the second approach, a polycrystalline Hastealloy™ substrate is coated with textured MgO buffer layer grown by ion beam assisted deposition (IBAD) and other subsequent buffer layers [4]. YBCO is deposited by metallo-organic chemical vapor deposition (MOCVD) on these substrates. In recent years, impressive progress has been made in the manufacturing of long lengths of YBCO coated conductors processed by using both the RABiTS™ substrates as well as IBAD substrates [6, 7]. Such long-length coated conductors are needed to make coils for rotating machinery and cables for electrical transmission. However, in high magnetic field applications such as MRI (Magnetic Resonance Imaging), SMES (Superconducting Magnetic Energy Storage), superconducting magnets and generators, etc., high J_c at high magnetic fields needs to be maintained. In the absence of flux pinning centers in the coated conductors, the magnetic flux lines will move due to Lorenz forces acting upon them at high fields. This motion causes dissipation, and losses will occur as a result. This lowers the J_c in coated conductors. Hence, it is important

Approved for public release; distribution unlimited

to incorporate flux pinning centers into coated conductors to improve the high-field J_c performance.

In addition to increasing the J_c, it is of importance to increase the J_e, the engineering critical current density. J_e is determined by dividing the critical current of a coated conductor (I_c) by the entire cross-section of a wire, including the thickness of the substrate, buffer layers, and metallic stabilizers, as well as the YBCO layer. The higher the J_c of a superconductor, the higher the resulting J_e of the coated conductor would be for similar thickness of buffers and substrate. Higher J_e conductors reduce the size of coils needed in the applications, and less of the superconductor material will be used, thereby reducing the total material and processing costs of the coils. Increasing J_c is also important in reducing the cost, size, and weight of coated conductors. The size and weight is of interest for airborne applications such as megawatt generators in future military aircraft [8].

Another problem faced with the coated conductor is the quench and instability of a coil winding during the operation. Local overheating will trigger normal zone propagation in the coil, quickly resulting in a quench and the attendant rapid boil-off of the liquid nitrogen, which can then damage the coil. The lower the operating current density of the coil, the less likely it is that the conductor will experience an incidence of quench. Hence, it is desirable to increase the J_c of coated conductors so that the coils can be run at reduced relative ratio of operating current density to critical current density level in order to avoid occurrences of quench and still be able to meet the required operating current levels.

One way to increase the J_c in coated conductors is to artificially introduce defects that pin the flux lines during the application of a magnetic field. Since the coherence length of YBCO is approximately 2 nm at 77 K, the defects necessary to serve as effective pinning centers need to be very small. In addition, the pinning centers must not disrupt the texture of the bulk YBCO lattice deposited on top of the buffer layers nor lower the critical transition temperature (T_c) of the superconductors. Although a slight depression in T_c from 90 K may be tolerated since the operating temperature is 77 K (i.e., the boiling temperature of liquid nitrogen), significant depression in T_c will result in inferior properties at 77 K. The pinning center material needs to be economically introduced, and the method of introduction needs to be compatible with the processing method of choice. It is further beneficial if the pinning centers can be introduced during the YBCO growth as opposed to during post-deposition processing. In recent years, significant progress has been made to improve the flux pinning in coated conductors [9], and some of the most recent developments are discussed below.

5.1.1
Types of Pinning Centers

Several types of pinning centers can be introduced into YBCO films for flux pinning enhancement. Some of them are

1) Crystalline Defects
2) Microstructural Defects

3) Rare Earth Doping
4) Second-phase Additions

5.1.1.1 Crystalline Defects

Crystalline defects such as stacking faults, dislocations, etc. can be introduced into the films by post-deposition anneals or by altering the growth conditions. For example, the high-temperature growth of YBCO by PLD deposition showed an increased number of defects such as stacking faults and dislocations [10, 11] that resulted in flux pinning enhancement.

5.1.1.2 Microstructural Defects

It has been suggested that pore surfaces can contribute to increase in flux pinning [12], and deposition on top of vicinal substrates or using second-phase particles was observed to lead to an increase in porosity. Also some defects were created by growing YBCO films on top of a surface decorated with nanoparticles (surface decoration). Nanoparticles of Ir or MgO are deposited initially on the substrates and then YBCO films were grown on top of these particles to grow films with defects that help to enhance J_c [13, 14]. In a separate study [15], nanoparticles of $BaTiO_3$ and $BaZrO_3$ were deposited by a solution-based technique onto a substrate prior to growing YBCO layers. Surface decoration techniques seem to help to create c-axis-correlated pinning centers, and J_c improvements were observed as a result of this. Threading low-angle grain boundaries induced by the surface-decorated nanoparticles were proposed to contribute to the enhanced pinning.

5.1.1.3 Rare Earth Doping

Rare earth ion doping may also help to improve the pinning by causing local variation of composition and associated defects. Rare earths element additions such as Nd, Sm, and Tb (minute amounts) were shown to improve the flux pinning properties in PLD YBCO films [16–18]. MOCVD films with Sm doping also showed considerable improvement in flux pinning enhancement. Chen *et al.* [19] reported that 17 vol.% of 10 nm sized $(Y,Sm)_2O_3$ nanoparticles were found in the films processed by Sm-doped YBCO by MOCVD and contributed to enhanced pinning. Recently $(Gd,Y)_2O_3$ nanostructures in MOCVD films were found in reel-to-reel MOCVD-processed coated conductors, and enhancements in critical currents were reported due to rare-earth doping [20]. Improvements due to Dy doping in MOD-deposited YBCO films were also reported [21]. High density of nanoparticles of $(Y, Dy)_2O_3$ 10–50 nm in diameter along with stacking faults and planar defects were observed, and these were proposed to contribute to enhance pinning [22, 23]. Eu-doped PLD films exhibited better magnetic field performance at low fields than pure YBCO at different orientations [24].

5.1.1.4 Second-Phase Additions

Nonsuperconducting second-phase additions of nano-dimensional size are another way to introduce pinning centers in YBCO. Both multilayers and random nanoparticulate pinning centers of a nonsuperconducting second-phase material can

be introduced depending upon the technique of deposition. While MOD and MOCVD are the most commonly used methods to process long-length conductors, PLD offers a quick screening tool to investigate pinning effects in YBCO films.

5.2
Pulsed-Laser Deposition (PLD)

Most of the pinning studies in the literature are done using the pulsed-laser deposition (PLD) method. Briefly, PLD is a physical vapor deposition technique in which an excimer laser is typically used to ablate the target in several short-duration pulses, and the evaporated material is made to condense onto a substrate heated to different temperatures. By using optimum temperatures of ambience, pressure, laser energy, substrate temperature, substrate-to-heater distance, and selection of the substrate materials, excellent quality YBCO films can be made. The targets used in PLD for flux pinning studies can be of the following types:

1) Alternate Targets
2) Pre-mixed Targets
3) Sectored Targets

5.2.1
Alternate Targets

Multilayers of YBCO and second-phase materials such as Y$_2$BaCuO$_5$, Y$_2$O$_3$ etc., can be deposited by alternatively ablating YBCO and second-phase targets that are periodically accessed during the deposition. This can be accomplished by controlling the laser beam's path, but most often is done by rotating the different targets in and out of the deposition zone. The thicknesses of the individual layers are controlled by how long each target is ablated. A discussion of the results of various films processed by this technique can be found in Refs [25–27].

5.2.2
Premixed Targets

Another way to deposit YBCO films with nanoparticles is to use a premixed YBCO target. For example, YBCO+BSO (BSO=BaSnO$_3$) [28] films were deposited by using a premixed target consisting of BSO second-phase additions and YBCO, which were mixed together in powder form prior to sintering of the final target. Other examples of premixed target PLD films include YBCO+BZO (BZO=BaZrO$_3$) [29–32], YBCO+RE$_3$TaO$_7$ (RE=Er, Gd, Yb) [33], YBCO+CaZrO$_3$ [32]. To study the effects of a systematic increase of pinning material content in YBCO films, targets would be mixed in powder form with the correct ratio of pinning material to bulk YBCO. An example of this type of study for BSO will be discussed later. In this study, different by-weight amounts of YBCO and BSO powders were mixed to make final target compositions with 2, 4, 10, and 20 mol% BSO in YBCO.
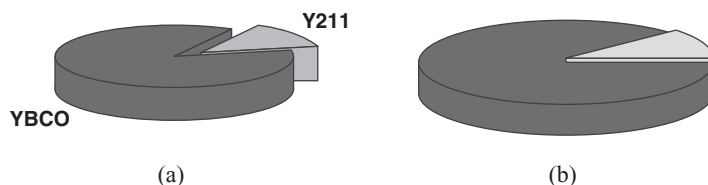
Figure 5.1 Schematic diagram of a PLD YBCO target with a small sector of a second phase such as Y_2BaCuO_5 or $BaSnO_3$ (a) Inserted type (b) thin sector on top type.

5.2.3
Sectored Target

A special pulsed laser ablation YBCO target with a second-phase material sector such as Y_2BaCuO_5 (Y211) or $BaSnO_3$ (BSO) was first used to make YBCO films with nanoparticle pinning centers [34, 35]. A thin sector piece (approx. 30°) cut from a disc is attached to the top surface of a YBCO target. As the target is rotated (at a speed of 15–20 rpm), the target is ablated at an approximate ratio of 11 pulses of YBCO to one pulse of the sector, resulting in the growth of a nanocomposite film. More than one sector can be used to deposit films with more than two different compositions in the films. The second-phase content can be varied by varying the sector size. It is also possible to use different sectors while maintaining a single YBCO target, and in this way the effect of second phases in films without changing the matrix composition can be investigated. Figure 5.1 shows a schematic of two types of such sectored targets.

5.3
Experimental Setup

Results discussed in the present chapter were obtained from films that were processed using either a sectored YBCO target or premixed target in pulsed-laser ablation. To make the targets, the powders were homogenously mixed using a mortar and pestle and then circular disks (1 inch diameter, ¼ inch thickness) were pressed using a hydraulic press. These disks were sintered at 920 °C for 170 h in air to get a final density > 90% of the theoretical density. A thin sector was cut and attached to the top surface of a YBCO target to make the sectored target. The premixed targets with different compositions were used as processed.

To process the samples, a Lambda Physik excimer laser (Model No. LPX 300, wavelength $\lambda = 248$ nm, KrF) was used to deposit the films at 780 °C using a 4 Hz repetition rate, 2 J cm^{-2} energy density in a Neocera PLD chamber containing oxygen at 300 mTorr pressure. Substrate-to-target distance was maintained at nearly 6 cm for all the depositions. All the films were annealed at 500 °C for 30 min in oxygen at 600 Torr pressure inside the chamber after the deposition was completed. Films of different thicknesses were deposited on (100) $LaAlO_3$ or buffered

metallic substrates, and the thickness was varied by increasing the duration of deposition.

The film microstructure was studied using a SIRION (FEI) ultra-high-resolution field emission scanning electron microscope (FE-SEM). The critical transition temperature (T_c) was measured by the AC susceptibility method. The magnetization J_c was measured using the hysteresis loop data acquired from a Quantum Design PPMS vibrating sample magnetometer (VSM) in H//c orientation. The Bean's model ($J_c = 20 \times \Delta M/[a(1-a/3b)]$), in which ΔM is the hysteresis in emu. cm^{-3} and a and b are the sample dimensions, was used to estimate J_c. Transport J_c measurements (angular dependence as well as in-field measurements) were taken on different thickness samples with a bridge length of 4 mm and width of 0.5 mm–0.02 mm. The thickness of the films was measured using a profilometer and verified with cross-sectional SEM.

5.4
Results and Discussion

5.4.1
YBCO Films Prepared Using a YBCO Sectored PLD Target with Y$_2$BaCuO$_5$ and BaSnO$_3$ Sectors

Figure 5.2 shows the magnetization J_c data (H//c) of YBCO+Y211 and YBCO+BSO films measured at various temperatures. It can be seen that the J_c of YBCO+Y211 films is lower than that of YBCO+BSO films at all the measured temperatures (77, 65, and 40 K). However, it should be noted that YBCO+Y211 films had better J_c
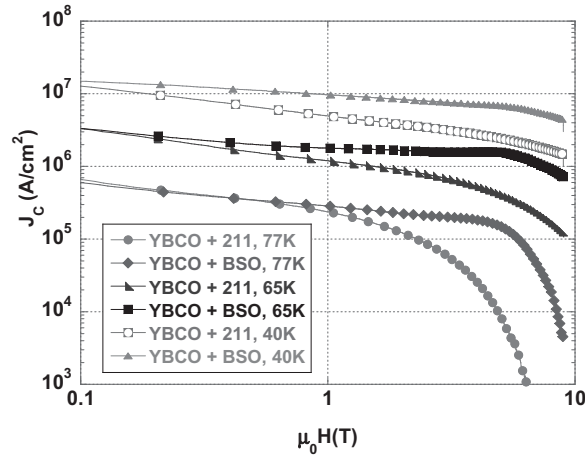

Figure 5.2 Magnetization J_c data (H//C) of YBCO+Y211 and YBCO+BSO films made by sector target method.

than regular YBCO films at these temperatures, but they do not have a J_c value as high as that of YBCO+BSO. The improvement in J_c is significant in YBCO+BSO films at higher fields, possibly because of the increase in the irreversibility field as well as the improved flux pinning.

Figure 5.3 shows a plan view SEM micrograph and a cross-sectional TEM micrograph of YBCO+Y211 films. Good dispersion of Y211 nanoparticles in the YBCO matrix can be seen. The bright particles in the SEM image and the dark particles in the TEM image correspond to the Y211 phase. The nanoparticles seem to be present throughout the thickness of the films. In addition to the nanoparticles, the YBCO+Y211 films also showed YBCO plane buckling due to the presence of these nanoparticles as evidenced by the cross-sectional TEM images published elsewhere [36]. In contrast to the YBCO+Y211 films, the YBCO+BSO films were found to have many BSO nanocolumns, as shown in a cross-sectional TEM image (Figure 5.4a as well as in Ref. [37]). In a plan view image, these nanocolumns appear to be nanoparticles, as shown in Figure 5.4b. It can be seen that the nanorods are uniform in diameter and are self-organized to be equidistant from each other. It is thought that a phase separation during the deposition and self-assembly are responsible for the nanorod growth. Strain due to lattice mismatch, texture, and deposition conditions seems to help to grow the nanocolumns with a certain constant diameter. Since BSO and YBCO are both perovskites, they tend to grow along the c-axis perpendicular to LAO substrate, and this resulted in the BSO nanocolumnar growth in a matrix of YBCO. A significant increase in J_c in H//c orientation due to these nanocolumns was observed as the magnetic flux line interaction with the nanocolumns is expected to be at maximum in this orientation. The nanorod diameter was found to be around 10–11 nm, and the density was estimated to be 3×10^{11} cm^{-2}. The normalized angular dependence of transport current data at 1 T shows that a peak only in YBCO+BSO samples is found at H//c, indicating the contribution of flux pinning due to nanocolumns in YBCO+BSO films in this direction.

5.4.2
Current Density and Alpha Value Variations with Temperature, and Dual Peaks in F_p Plots of YBCO+BSO Samples

The alpha values at 77 K were found to be smaller for YBCO+BSO films than those for films of YBCO or YBCO+Y211. Typically, for undoped YBCO an alpha value of 0.5 at 77 K is noted [38]. The alpha values of YBCO+Y211 samples were found to be around 0.4–0.5, whereas for YBCO+BSO films they were found to be 0.2–0.3. In addition, alpha values of YBCO+BSO samples were found to decrease with temperature to a value as low as 0.1 at 20 K, as shown in Figure 5.5.

The J_c value variations with temperature for YBCO+BSO films are shown in Figure 5.6. This figure includes additional J_c data taken at temperatures other than those shown in Figure 5.2, as some applications may need to be carried out at lower temperatures. As expected, the J_c continued to increase as the temperature was lowered and was found to be higher than that for YBCO or YBCO+Y211 films.
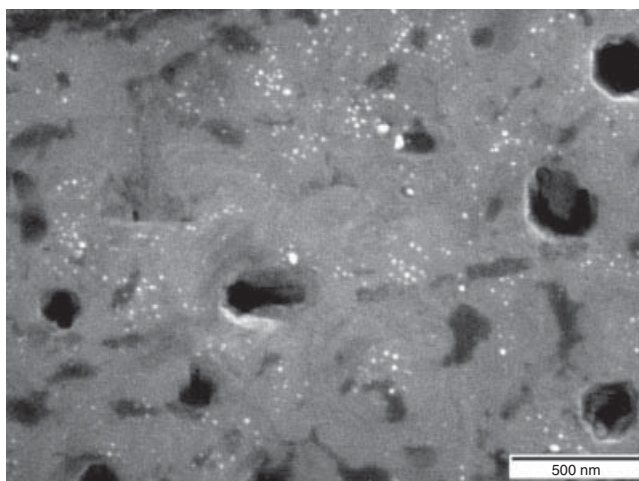
(a)
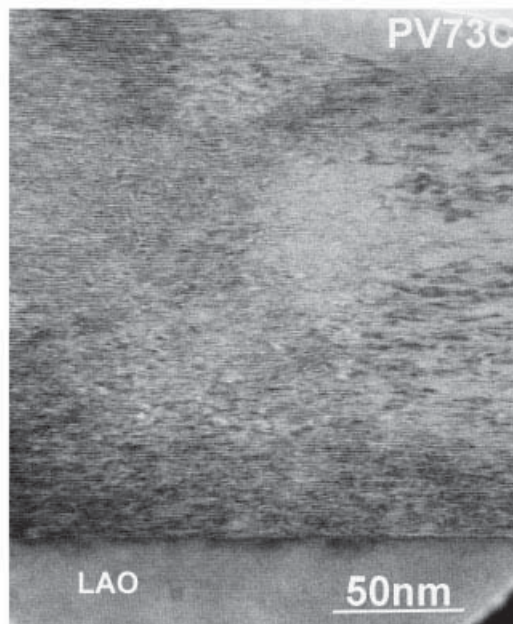
(b)

Figure 5.3 (a) SEM micrograph of YBCO+Y211 film made by sectored target approach. (b) Cross-sectional TEM micrograph of YBCO+Y211 film made by sectored target approach.

It was found that the flux pinning force increases in YBCO+BSO films as compared to YBCO or YBCO+Y211 films, showing values as high as 18 GN cm^{-3} at 77 K for a 300 nm thick film (Figure 5.7). Flux pinning force maxima ($F_{p\,max}$) higher than this value are possible in thicker films, as discussed later. It can be seen that the peak shifts to higher fields, and sometimes clearly discernible dual peaks were

(a)

(b)
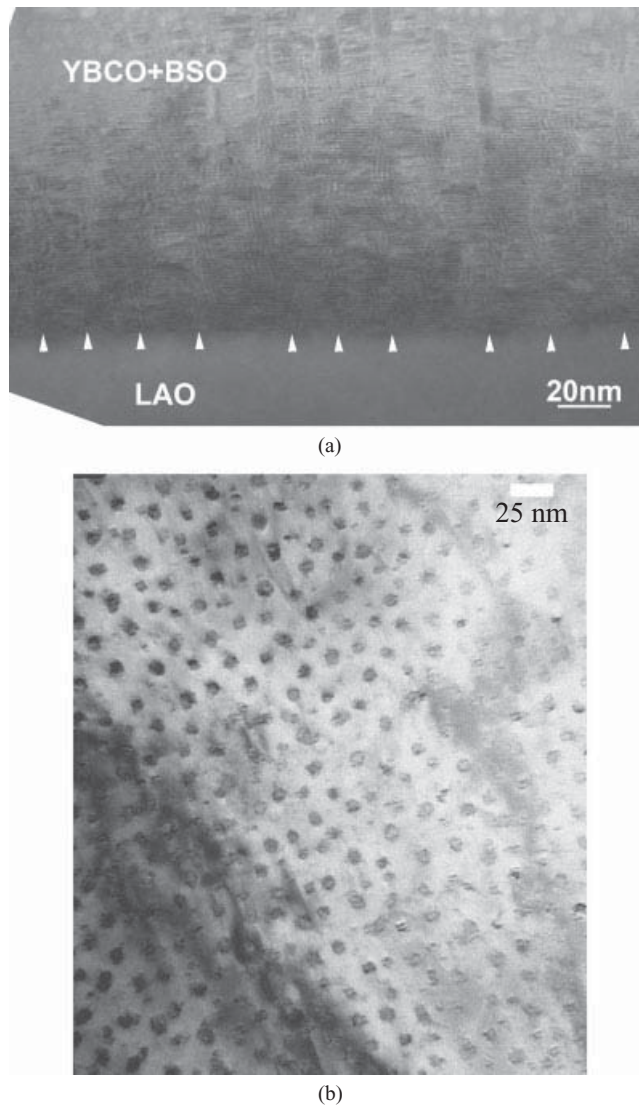
Figure 5.4 (a) Cross-sectional TEM micrograph of a YBCO+BSO film made by sectored target approach. (b) Plan view TEM micrograph of a YBCO+BSO film made by sector target approach.

also observed in YBCO+BSO samples. A shoulder at low fields followed by a peak at the higher fields was observed. Such dual peaks were not observed in YBCO or YBCO+Y211 samples. It was observed that the peak intensity is lowered as the peak shifts to higher fields in YBCO+BSO samples. The presence of dual peaks can be ascribed to dual pinning mechanisms that may be operative, as discussed in Ref. [39].
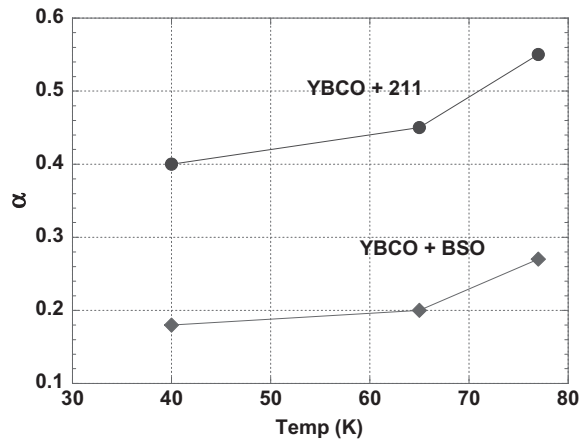
9

Figure 5.5 Alpha values of YBCO+Y211 and YBCO+BSO films at different temperatures.
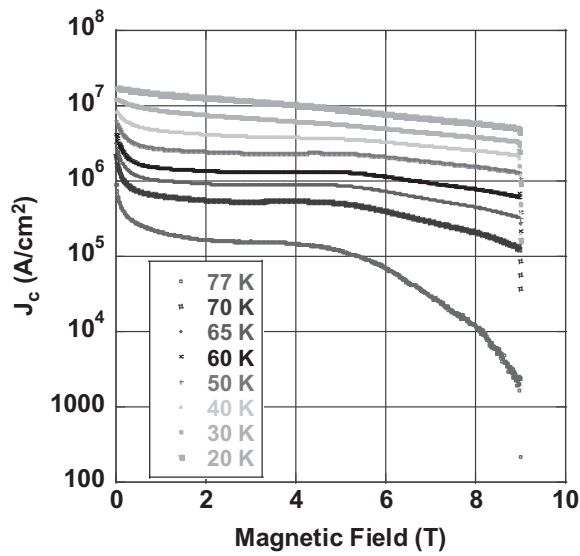

Figure 5.6 Magnetization J_c of YBCO+BSO films at various temperatures.

5.4.3
High-Quality YBCO+BSO Thick Films

In the literature, it is reported that when thickness is increased, a gradual drop in J_c is observed in regular YBCO films [9]. To overcome this problem Foltyn *et al.* proposed thin YBCO layers separated by thin CeO$_2$ layers, and by using this approach they achieved 4 MA cm^{-2} J_c at 75 K self field in films as thick as 3.5 μm
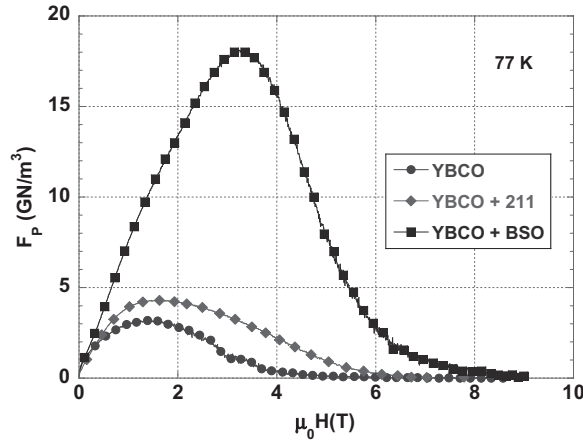
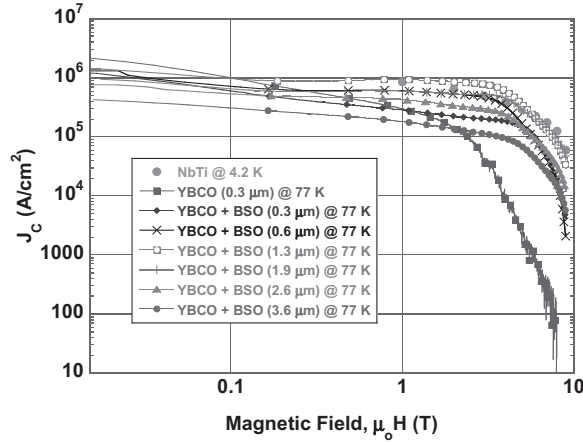**Figure 5.7** F_p plots of YBCO+BSO, YBCO+211, and YBCO films at 77 K.

Figure 5.8 J_c of YBCO+BSO films with different thicknesses as a function of magnetic field.

[40]. In order to investigate whether the BSO nanocolumns help to maintain high J_c in thick films, several YBCO+BSO films with different thicknesses were grown. The YBCO+BSO thick films were deposited by simply increasing the duration of deposition while all other processing parameters were kept constant. All the films presented here were made using a YBCO target with a 30-degree BSO sector. As shown in Figure 5.8, all the films with different thicknesses were found to maintain higher J_c at high fields than those observed with regular YBCO. It can also be seen that at 77 K and high magnetic fields, the J_c of 1.9 μm and 1.3 μm thick YBCO+BSO films match well with that of NbTi wires at 4.2 K. In the YBCO+BSO films, the J_c actually improved as the thickness was increased from 300 nm to 1 μm.
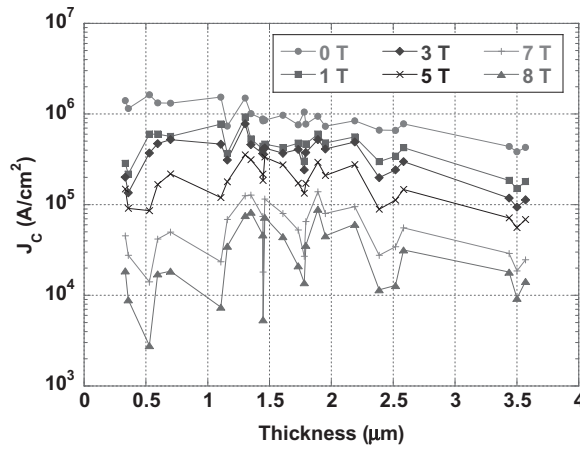
Figure 5.9 J_c of films with different thicknesses at different magnetic fields plotted as a function of thickness.
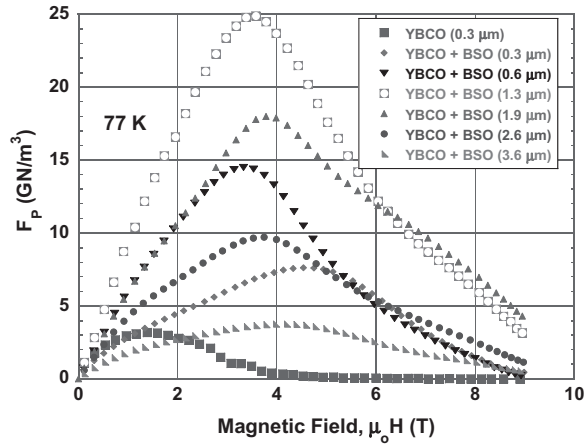

Figure 5.10 Flux pinning force (F_p) data for various samples with different thicknesses.

Figure 5.9 shows the J_c at different fields plotted as a function of thickness. It can be seen that 3.5 μm thick films can be formed with a similar J_c to that for a 300 nm thick film at 8 T, showing no degradation in J_c. Figure 5.10 shows the flux pinning force (F_p) data for various samples with different thicknesses, and it can be seen that an $F_{p\,max}$ as high as 25 GN cm^{-3} can be obtained in these films. $F_{p\,max}$ values seem to depend on the position, F_p decreasing as the peak position is moved to higher fields. TEM images show long BSO nanocolumns that extend throughout the thickness of the films, as shown in Figure 5.11. The density of the
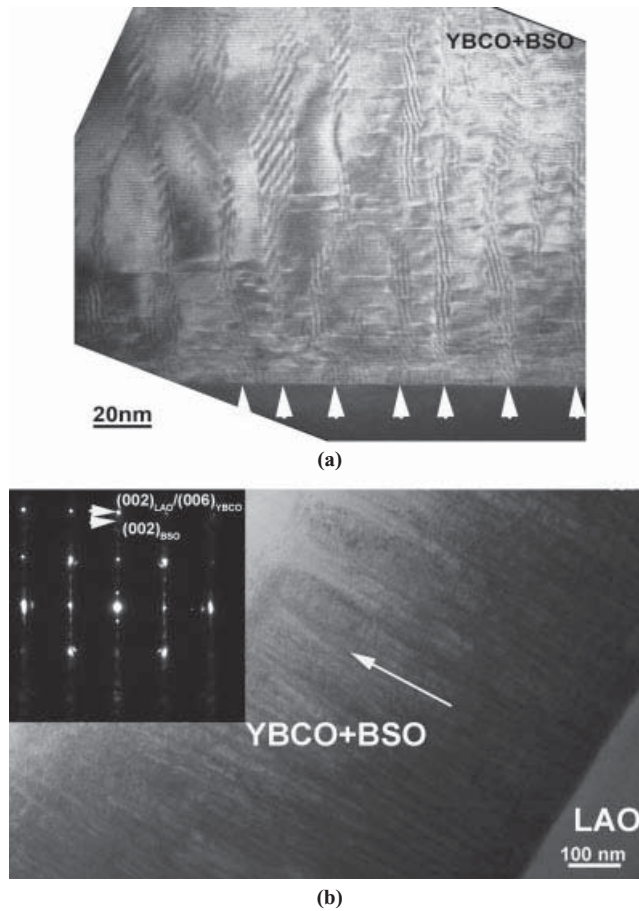
Figure 5.11 Cross-sectional TEM images of YBCO+BSO thick films at different magnifications showing that the BSO nanocolumns extend throughout the thickness.

nanocolumns was approximately $2.5 \times 10^{11}\,\text{cm}^{-2}$, and the average size was 10–11 nm. As compared to $BaZrO_3$, nanocolumns of BSO seem to grow straight, and, as a result of this microstructure, thick films continue to have higher J_c [41]. The strain between BSO and YBCO seems to help to grow such nanocolumns [42]. In addition, thick films showed some regions of very ordered and parallel nanocolumns, as shown earlier in Figure 5.12. These straight nanocolumns, which are ordered in some places, are thought to be responsible for improved J_c values in thick films.

However, as the thickness was increased beyond $3.5\,\mu\text{m}$ with the present set of deposition conditions, a decreased J_c in films was observed. Although all the thick films had structurally well-defined nanocolumns (seen as nanoparticles in plan view) as shown in high magnification SEM images (Figure 5.13), the
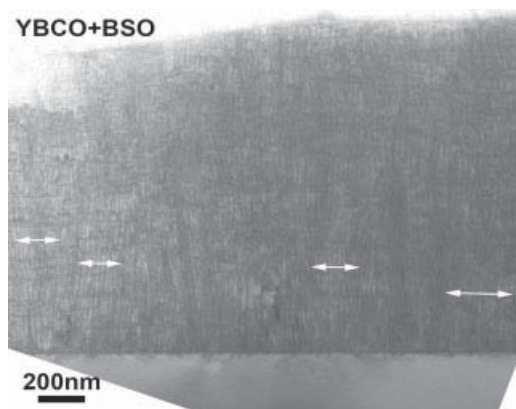
Figure 5.12 Cross-sectional TEM images of YBCO +BSO thick films showing the ordering of nanocolumns as shown by arrow marks.
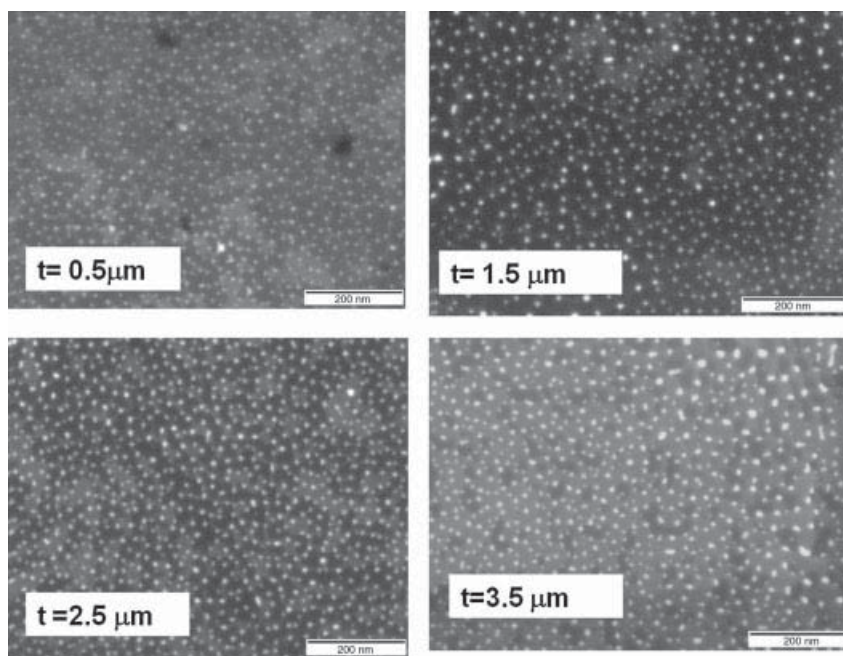

Figure 5.13 High-resolution scanning electron images of YBCO+BSO thick films with different thicknesses (denoted by 't') showing the planar view of the BSO nanorods.
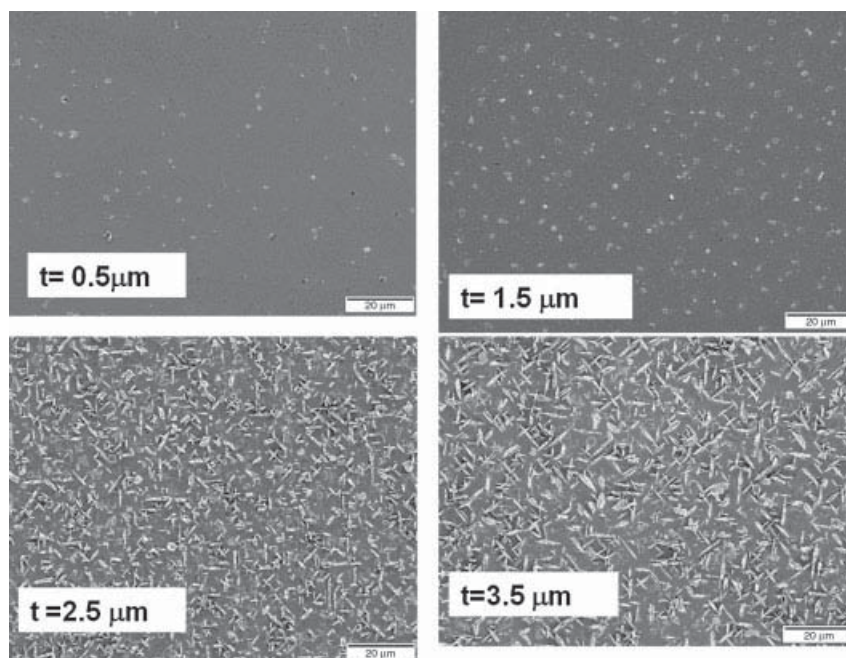
Figure 5.14 Low magnification SEM images of YBCO+BSO thick film showing an increase in the amount of misoriented grains as the thickness was increased.

lower magnification images (Figure 5.14) of these films showed roughening of the films due to the growth of other orientation (such as *a* axis) grains. X-ray diffraction data taken on thick films indicated that the (103) orientation grains were also present in these films (as shown in Figure 5.15). The increased number of misoriented grains is believed to be due to decreased substrate temperature as the thickness was increased. However, this occurs in much thinner films, typically starting at one micron in the YBCO-only films. Because of the increased number of these misoriented grains, the J_c of films with more than 3.5 μm can be expected to decrease. If a correct growth temperature can be maintained to avoid the formation of misoriented grains, much thicker films with the same quality as thin YBCO+BSO films can be made with improved properties. Even so, the addition of the BSO nanocolumns apparently delays the formation of the misoriented growth until significantly thicker films are produced.

5.4.4
YBCO+BSO Effects of Concentrations

To investigate the effect of concentration on properties, YBCO films were made using different targets with varying BSO contents. Targets with 2, 4, 10, and
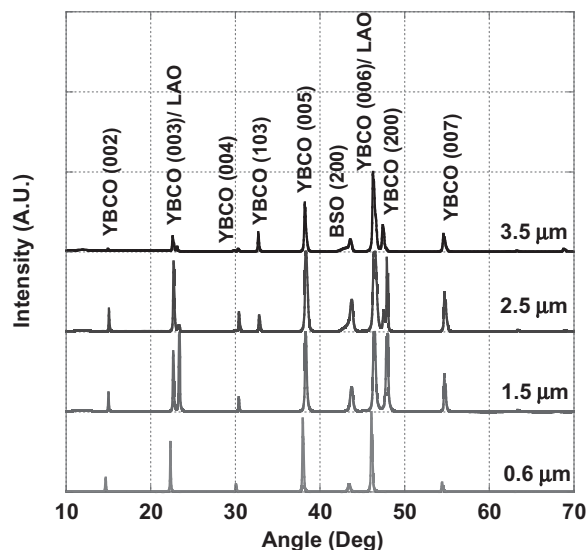
Figure 5.15 X-ray diffraction patterns of YBCO+BSO thick films showing the BSO (100), YBCO (100) peaks in all samples. An increase in YBCO (103) can be seen as thickness was increased.

20 mol% BSO additions were used to make films, and flux pinning and microstructural variations were studied. The cross-sectional TEM images show that the BSO nanocolumns increased in density as the BSO content was increased, while the diameter remained the same (ca. 8–10 nm, Figure 5.16). Both plan views and side views of samples are shown in Figure 5.16. The nanocolumns appear as nanoparticles in the plan view. Since the columns are continuous, the BSO concentration in the films is difficult to estimate using normal image analysis assumptions to estimate size and volume from the area fractions. Therefore, the descriptive concentrations in the present discussion are the starting composition of the targets rather than the actual compositions in the films. X-ray diffraction data taken on these films showed c axis orientation for both YBCO and BSO [28]. It was observed that a high quality YBCO film continues to grow around the nanocolumns. BSO nanocolumns nucleate at the substrate and grow through the entire thickness of the films. Flux pinning enhancement through BSO additions has also recently been confirmed by other groups. Mele *et al.* [43] reported F_p values for YBCO+BSO films of 28.3 GN m^{-3} at 2 T at 77 K and also compared with BZO nanorods in a YBCO matrix [44] and suggested that BSO nanorods grow straighter than BZO nanorods, which tend to splay, and as result BSO serves as a better pinning center. Teranishi *et al* [45] reported that BZO and BSO nanorods form in ErBa$_2$Cu$_3$O$_{7-x}$ as well with a diameter of 10–20 nm, and BSO nanorods provided more effective pinning than BZO in applied magnetic fields, showing higher J_c in ErBCO+BSO films than ErBCO+BZO. M. Tanaka *et al.* [46] reported the formation of BSO
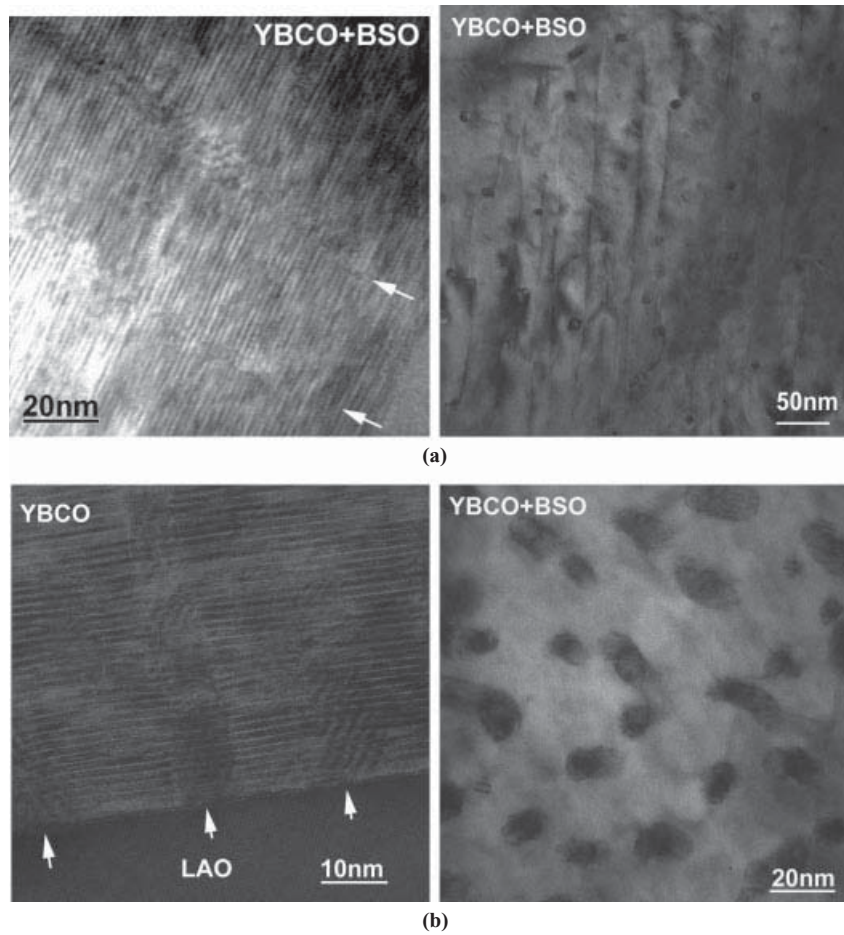
Figure 5.16 Plan view and cross-sectional view of TEM images of YBCO+BSO samples with two different levels of BSO content (a) 2 mol% and (b) 20 mol%.

nanorods of 20 nm diameter in $NdBa_2Cu_3O_{7-x}$. Based on these results it appears that BSO nanorod formation is independent of the RE in REBCO.

As the BSO content was increased, the J_c (especially at higher fields) of the films was found to be increased up to the highest BSO contents (20 mol%). However, the low-field J_c degraded slightly in the heavily doped samples. The optimum level of doping was found to be 10 mol% (as shown in Figure 5.17), which showed enhanced J_c at all the field levels (0–9 T) tested.

Alpha values of these samples are shown in Table 5.1. It can be seen that samples with increased BSO content had lower values, decreasing from the usual alpha value of 0.5 for YBCO to as low as 0.26 for 20 mol% BSO doped samples. The lower alpha value found in the 20 mol% BSO doped samples is consistent
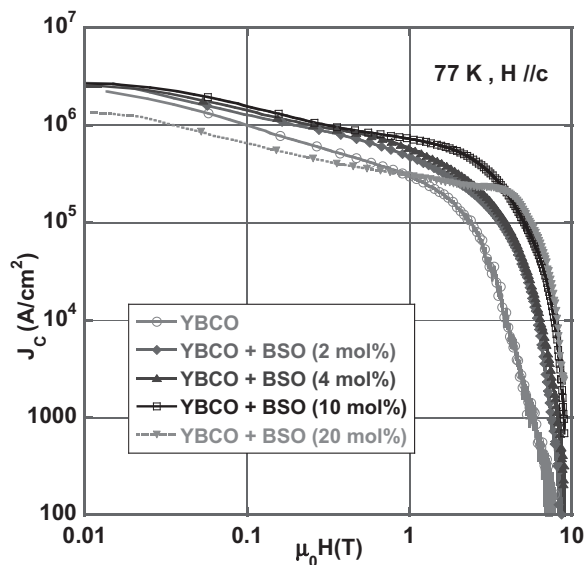
Figure 5.17 Magnetization J_c of YBCO+BSO samples with different amounts of BSO content.

Table 5.1 Alpha values of YBCO films with varying amounts of BSO content.

Varying BSO Content	Average Alpha Values at 77 K
YBCO	0.50
YBCO + BSO (2 mol%)	0.40
YBCO + BSO (4 mol%)	0.36
YBCO + BSO (10 mol%)	0.31
YBCO + BSO (20 mol%)	0.26

with the values observed in the samples made using the 30-degree sectored target approach, which generally yields samples with a similar volume fraction to the 20 mol% BSO in the films.

5.4.5
YBCO+BSO Films on Coated-Conductor Technical Substrates (Buffered Metallic Substrates)

YBCO+BSO films were also deposited on Y$_2$O$_3$/YSZ/CeO$_2$-buffered Ni-5 wt.%W biaxially textured metallic substrates to investigate whether similar improvements to those seen on the single crystal substrates could be observed on technical substrates that are presently used for long-length manufacturing. A high-resolution
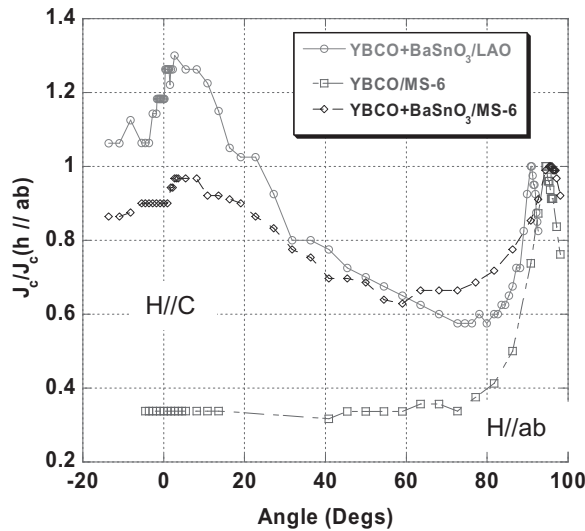
18

Figure 5.18 Transport current density data of YBCO+BSO film on a LaAlO₃ and a buffered
metallic substrate as compared to YBCO film on a metallic substrate. (LAO = LaAlO₃,
MS-6 = buffered metallic substrate)

SEM micrograph on such a sample shows that microstructure similar to that seen
on the YBCO+BSO coatings on $LaAlO_3$ substrates (shown before) can be obtained.
This indicates that the BSO nanocolumns can grow independently of the substrate
used, provided that similar deposition conditions are used. Transport current data
at a 1 T field on such samples showed that $J_c \approx 6 \times 10^5\,A\,cm^{-2}$ at 77 K both at H//c
and H//ab can be obtained [37]. The data suggest that improvements as seen in
the films deposited on $LaAlO_3$ substrates can also be observed in YBCO+BSO
samples on coated-conductor substrates. Flux pinning enhancements due to
c-axis-correlated defects often result in increased J_c in H//C orientations as
compared to H//ab orientation. Civale *et al.* [47] proposed that because of intrinsic
pinning due to the layered structure of YBCO a peak at H//ab orientation appears,
and because of c-axis-correlated pinning due to columnar defects, a peak in H//c
orientation results. Figure 5.18 shows the normalized transport current data of
YBCO+BSO samples as compared to a YBCO sample processed on a metallic
substrate. The improvement in J_c at H//c is higher than that of of J_c at H//ab,
indicating that nanocolumns similar to those seen in the samples processed on
single-crystal substrates are present in the films deposited on metallic substrates
as well. These columns are c-axis oriented and contribute toward enhancing the
critical current density in H//C. The pinning due to the columnar defects appears
to be more than the intrinsic pinning due to the layered structure of YBCO.
YBCO+BZO samples also showed similar peaks in J_c at H//C and J_c at H//ab
orientations due to the presence of BZO nanorods [48, 49] in YBCO+BZO samples,
corroborating the data observed with YBCO+BSO samples. Recently, the sectored
target method was used by other groups to make films with YBCO+Y_2O_3 [50] and

YBCO+BaZrO$_3$+Y$_2$O$_3$ [51] compositions. These samples also showed the formation of nanocolumns and accordingly improved properties. Other studies focused on comparing the BZO and BSO in YBCO materials and indicated that BSO performs better than BZO

5.5
Summary

It is shown that YBCO films with BaSnO$_3$ (BSO) nano-additions, made with either a sectored target or with a premixed target using pulsed-laser deposition (PLD), have a much greater improvement in J_c at the higher fields with an H//c orientation. More than two orders of magnitude improvement in J_c was observed as compared to undoped or similarly processed Y$_2$BaCuO$_5$ (Y211) doped samples at magnetic fields higher than 5 T. The improvement was found to be due to the formation of BSO nanocolumns 8–10 nm in diameter in the films. These nanocolumns nucleate at the interface and subsequently grow perpendicular to the substrate while allowing high-quality YBCO to grow around them. Although similar processing conditions were used, Y211 formed nanoparticles, whereas BSO formed nanocolumns in the YBCO because of the crystal structure match between BSO and YBCO (both are perovskites) and appropriate lattice strain and suitable deposition conditions. The BSO content was also systematically increased from 2 to 20 mol% by using premixed targets of YBCO and BSO to explore the effects of BSO content variation in YBCO. It was shown that even with 20 mol% BSO addition; films can be grown without a significant decrease in critical transition temperature (T_c). While the diameter of the nanocolumns remained at 8–10 nm, the distance between them decreased from 50 nm to 20 nm as the concentration was increased from 2 mol% to 20 mol%, resulting in an increase in the number density. An overall improvement at both low and high fields was observed in samples of YBCO+10 mol% BSO. BSO nanocolumns were also found to help maintain a high critical current density ($J_c > 10^4$ A cm^{-2}, at 8 T) in thick films made by a sectored target and showed no degradation in J_c at the higher fields when the thickness was increased from 300 nm to 3 μm. Also $F_{p\ max}$ values of more than 25 GN m^{-3} at 77 K were noted in the YBCO+BSO films with thickness >1 μm. The F_p peak position was found to be shifted to higher fields (>4 T), and two clearly distinguishable peaks were observed in some of the F_p plots. The YBCO+BSO films deposited on buffered metallic substrates showed similar improvements as seen on the single-crystal substrates, indicating that the BSO nano-additions can be introduced on polycrystalline buffer layers as used in coated conductors. Unlike BaZrO$_3$, BSO seems to allow higher relative amounts of additions to YBCO without significantly depressing the T_c value. The BSO nanocolumns seem to grow as solid nanorods as opposed to stacked individual nanoparticles. In addition, they were found to grow vertically straight and hence help to improve the J_c at high fields by several orders of magnitude in thick films making BSO attractive for coated conductors.

Acknowledgments

References

1 Larbalestier, D., Gurevich, A., Feldmann, D.M., and Polyanskii, A. (2001) *Nature*, **414**, 368.

2 Goyal, A., Lee, D.F., List, F.A., Specht, E.D., Feenstra, R., Paranthaman, M., Cui, X., Lu, S.W., Martin, P.M., Kroeger, D.M., Christen, D.K., Kang, B.W., Norton, D.P., Park, C., Verebelyi, D.T., Thompson, J.R., Williams, R.K., Aytug, T., and Cantoni, C. (2001) *Physica C*, **357–360**, 903.

3 Li, X., Rupich, M.W., Kodenkandath, T., Huang, Y., Zhang, W., Siegal, E., Verebelyi, D.T., Schoop, U., Nguyen, N., Thieme, C., Chen, Z., Feldman, D.M., Larbalestier, D.C., Holesinger, T.G., Civale, L., Jia, Q.X., Maroni, V., and Rane, M.V. (2007) *IEEE Trans. Supercond.*, **17**, 3553.

4 Xiong, X., Lenseth, K.P., Reeves, J.L., Rar, A., Qiao, Y., Schmidt, R.M., Chen, Y., Li, Y., Xie, Y.-Y., and Selvamanickam, V. (2007) *IEEE Trans. Supercond.*, **17**, 3375.

5 Aytug, T., Paranthaman, M., Heatherly, L., Zuev, Y., Zhang, Y., Kim, K., Goyal, A., Maroni, V.A., Chen, Y., and Selvamanickam, V. (2009) *Supercond. Sci. Technol.*, **22**, 015008.

6 Malozemoff, P., Fleshler, S., Rupich, M., Thieme, C., Li, X., Zhang, W., Otto, A., Maguire, J., Folts, D., Yuan, J., Kraemer, H.-P., Schmidt, W., Wohlfart, M., and Neumueller, H.-W. (2008) *Supercond. Sci. Technol.*, **21**, 034005.

7 Selvamanickam, V., Chen, Y., Xiong, X., Xie, Y.Y., Reeves, J.L., Zhang, X., Qiao, Y., Lenseth, K.P., Schmidt, R.M., Rar, A., Hazelton, D.W., and Tekletsadik, K. (2007) *IEEE Trans. Appl. Supercond.*, **17**, 3231.

8 Barnes, P.N., Sumption, M.D., and Rhoads, G.L. (2005) *Cryogenics*, **45**, 670.

9 Foltyn, S.R., Civale, L., MacManus-Driscoll, J.L., Jia, Q.X., Maiorov, B., Wang, H., and Maley, M. (2007) *Nat. Mater.*, **6**, 631.

10 Wang, J., Kwon, J.H., Yoon, J., Wang, H., Haugan, T.J., Baca, F.J., Pierce, N.A., and Barnes, P.N. (2008) *Appl. Phy. Lett.*, **92**, 082507.

11 Feldmann, D.M., Ugurlu, O., Maiorov, B., Stan, L., Holesinger, T.G., Civale, L., Foltyn, S.R., and Jia, Q.X. (2007) *Appl. Phys. Lett.*, **91**, 162501.

12 Emergo, R.L.S., Wu, J.Z., Haugan, T.J., and Barnes, P.N. (2005) *Appl. Phys. Lett.*, **87**, 232503.

13 Aytug, T., Paranthaman, M., Gapud, A.A., Kang, S., Christen, H.M., Leonard, K.J., Martin, P.M., Thompson, J.R., and Christen, D.K. (2005) *J. Appl. Phys.*, **98**, 114309.

14 Matsumato, K., Horide, T., Ichinose, A., Horii, S., Yoshida, Y., and Mukaida, M. (2005) *Jpn. J. Appl. Phys. A*, **449**, L246.

15 Aytug, T., Paranthaman, M., Leonard, K.J., Kim, K., Ljaduola, A.O., Zhang, Y., Tuncer, E., Thomson, J.R., and Christen, D.K. (2008) *J. Appl. Phys.*, **104**, 043906.

16 Varanasi, C., Biggers, R., Maartense, I., Dempsey, D., Peterson, T.L., Solomon, J., McDaniel, J., Kozlowski, G., Nekkanti, R., and Oberly, C.E. (1998) Proceed. Mater. Res. Soc. Advances in Laser Ablation of Materials Symposium (eds R.K. Singh, D. Lowndes, D.B. Chrisey, E. Fogarassy, and J. Narayan), Materials Research Society, Warrendale, PA, p. 263.

17 MacManus-Driscoll, J.L., Foltyn, S.R., Jia, Q.X., Wang, H., Serquis, A.,

Maiorov, B., Civale, L., Lin, Y., Hawley, M.E., Maley, M.P., and Peterson, D.E. (2004) *Appl. Phys. Lett.*, **84**, 5329.

18 Barnes, P.N., Kell, J.W., Harrison, B.C., Haugan, T.J., Varanasi, C.V., Rane, M., and Ramos, F. (2006) *Appl. Phys. Lett.*, **89**, 012503.

19 Chen, Z., Feldmann, D.M., Song, X., Kim, S.I., Gurevich, A., Reeves, J.L., Xie, Y.Y., Selvamanickam, V., and Larbalestier, D.C. (2007) *Supercond. Sci. Technol.*, **20**, S205.

20 Chen, Y., Selvamanickam, V., Zhang, Y., Zuev, Y., Cantoni, C., Specht, E., Paranthaman, M., Aytug, T., Goyal, A., and Lee, D. (2009) *Appl. Phys. Lett.*, **94**, 062513.

21 Goyal, A., Li, J., Martin, P.M., Gapud, A., Specht, E.D., Paranthaman, M., Li, X., Zhang, W., Kodenkandath, T., and Rupich, M.W. (2007) *IEEE Trans. Appl. Supercond.*, **17**, 3340.

22 Long, N., Strickland, N., Chapman, B., Ross, N., Xia, J., Li, X., Zhang, W., Kodenkandath, T., Huang, Y., and Rupich, M. (2005) *Supercond. Sci. Technol.*, **18**, S405.

23 Xia, J.A., Long, N.J., Strickland, N.M., Hoefakker, P., Talantsev, E.F., Li, X., Zhang, W., Kodenkandath, T., Huang, Y., and Rupich, M.W. (2007) *Supercond. Sci.Technol.*, **20**, 880.

24 Zhou, H., Mairov, B., Wang, H., MacManus-Driscoll, J.L., Holesinger, T.G., Civale, L., Jia, Q.X., and Foltyn, S.R. (2008) *Supercond. Sci. Technol.*, **21**, 025001.

25 Haugan, T.J., Barnes, P.N., Wheeler, R., Meisenkothen, F., and Sumption, M. (2004) *Nature*, **430**, 867.

26 Campbell, T.A., Haugan, T.J., Maartense, I., Murphy, J., Brunke, L., and Barnes, P. (2005) *Physica C*, **423**, 1.

27 Haugan, T., Barnes, P.N., Maartense, I., Cobb, C.B., Lee, E.J., and Sumption, M. (2003) *J. Mater. Res*, **18**, 2618.

28 Varanasi, C.V., Burke, J., Brunke, L., Wang, H., Lee, J.H., and Barnes, P.N. (2008) *J. Mater. Res.*, **23**, 3363.

29 MacManus-Driscoll, J.L., Foltyn, S.R., Jia, Q.X., Wang, H., Serquis, A., Civale, L., Maiorov, B., Hawley, M.E., Maley, M.P., and Peterson, D.E. (2004) *Nat. Mater.*, **3**, 439.

30 Kang, S., Goyal, A., Li, J., Gapud, A.A., Martin, P.M., Heatherly, L., Thomson, J.R., Christen, D.K., List, F.A., Paranthaman, M., and Lee, D.F. (2006) *Science*, **311**, 1911.

31 Perula, M., Huhtinen, H., Shakhov, M.A., Traito, K., Steanov, Yu.P., Safonchik, M., Paturi, P., Tse, Y.Y., Palai, R., and Laiho, R. (2007) *Phys. Rev. B*, **75**, 184524.

32 Kang, S., Goyal, A., Li, J., Martin, P., Ijaduola, A., Thomson, J.R., and Paranthaman, M. (2007) *Physica C*, **457**, 41.

33 Harrington, S.A., Durrell, J.H., Maiorov, B., Wang, H., Wimbush, S.C., Kursumovic, A., Lee, J.H., and MacManus-Driscoll, J.L. (2009) *Supercond. Sci. Technol.*, **22**, 022001.

34 Varanasi, C., Barnes, P.N., Burke, J., Carpenter, J., and Haugan, T.J. (2005) *Appl. Phys. Lett.*, **87**, 262510.

35 Varanasi, C.V., Barnes, P.N., Burke, J., Brunke, L., Maartense, I., Haugan, T.J., Stinzianni, E.A., Dunn, K.A., and Haldar P. (2006) *Supercond. Sci. Technol.*, **19**, L37.

36 Varanasi, C.V., Burke, J., Brunke, L., Lee, J.H., Wang, H., and Barnes, P.N. (2009) *IEEE Trans. Appl. Supercond.*, **19(3)**, 3152.

37 Varanasi, C.V., Burke, J., Brunke, L., Wang, H., Sumption, M., and Barnes, P.N. (2007) *J. Appl. Phys.*, **102**, 063909.

38 Gapud, A., Kumar, D., Viswanathan, S.K., Cantoni, C., Varela, M., Abiade, J., Pennycook, S.J., and Christen, D.K. (2005) *Supercond. Sci. Technol.*, **18**, 1502.

39 Varanasi, C.V., Barnes, P.N., and Burke, J. (2007) *Supercond. Sci. Technol.*, **20**, 1071.

40 Foltyn, S.R., Wang, H., Civale, L., Jia, Q.X., Arendt, P.N., Mairov, B., Li, Y., and Maley, M.P. (2005) *Appl. Phys. Lett.*, **87**, 162505.

41 Varanasi, C.V., Burke, J., and Barnes, P.N. (2008) *Appl. Phys. Lett.*, **93**, 092501.

42 Rodriguez, J.P., Barnes, P.N., and Varanasi, C.V. (2008) *Phys. Rev. B*, **78**, 052505-1-4.

43 Mele, P., Matsumoto, K., Horide, T., Ichinose, A., Mukaida, M., Yoshida, Y., Horii, S., and Kita, R. (2008) *Supercond. Sci. Technol.*, **21**, 032002.

44 Mele, P., Matsumato, K., Ichinose, A., Mukaida, M., Yoshida, Y., Horii, S., and Kita, R. (2008) *Supercond. Sci. Technol.*, **21**, 125017.

45 Teranishi, R., Yasunaga, S., Kai, H., Yamada, K., Mukaida, M., Mori, N., Fujiyoshi, T., Ichinose, A., Horii, S., Matsumoto, K., Yoshida, Y., Kita, R., and Awaji, S. (2008) *Physica C*, **468**, 1522.

46 Tanaka, Y., Mukaida, M., Teranishi, R., Yamada, K., Ichinose, A., Matsumaoto, K., Horii, S., Yoshida, Y., Kita, R., Fujiyoshi, T., and Mori, N. (2008) *Physica C*, **468**, 1864.

47 Civale, L., Maiorov, B., Serquis, A., Willis, J.O., Coulter, J.Y., Wang, H., Jia, Q.X., Arendt, P.N., MacManus-Driscoll, J.L., Maley, M.P., and Foltyn, S.R. (2004) *Appl. Phys. Lett.*, **84**, 2121.

48 Civale, L., Mairov, B., Serquis, A., Foltyn, S.R., Jia, Q.X., Arendt, P.N., Wang, H., Willis, J.O., Coulter, J.Y., Holesinger, T.G., MacManus-Driscoll, J.L., Rupich, M.W., Zhang, W., and Li, Z. (2004) *Physica C*, **412–414**, 976.

49 Wee, S.H., Goyal, A., Zuev, Y., and Cantoni, C. (2008) *Supercond. Sci. Technol.*, **21**, 092001.

50 Mele, P., Matsumato, K., Horide, T., Ichinose, A., Mukaida, M., Yoshida, Y., Horii, S., and Kita, R. (2008) *Supercond. Sci. Technol.*, **21**, 015019.

51 Ichinose, A., Mele, P., Horide, T., Matsumato, K., Goto, G., Mukaida, M., Kita, R., Yoshida, Y., and Horii, S. (2008) *Physica C*, **468**, 1627.